Available online at www.sciencedirect.com
ScienceDirect
Trans. Nonferrous Met. Soc. China 31(2021) 426−437
Transactions of Nonferrous Metals Society of China
www.tnmsc.cn

Effects of solution treatment on microstructure and tensile properties of as-cast alloy 625

Fei YANG[1,2], Jie-shan HOU[1], Chang-shuai WANG[1], Lan-zhang ZHOU[1]

1. Institute of Metal Research, Chinese Academy of Sciences, Shenyang 110016, China;
2. School of Materials Science and Engineering, University of Science and Technology of China, Hefei 230026, China

Received 8 April 2020; accepted 2 December 2020

Abstract: Effects of solution treatment between 1050 and 1250 °C on microstructure and tensile properties of as-cast alloy 625 were investigated. The microstructure and solidification characteristics of the alloy were studied by SEM, EDS, EPMA and DTA. The results showed that the solidification sequence of the alloy should be written as $L \rightarrow L+\gamma \rightarrow L+\gamma+\text{MC} \rightarrow L+\gamma+\text{MC}+\gamma/\text{Laves} \rightarrow \gamma+\text{MC}+\gamma/\text{Laves}$. After solution treatment at 1225 and 1250 °C, incipient melting of Laves phase was observed. The ultimate tensile strength decreased monotonically with the increase of solution treatment temperature, and the yield strength had no significant variation. The elongation increased slightly at first and then reached a minimum value at 1250 °C. The fracture mechanism changed from transgranular mode to intergranular mode after solution at 1250 °C for the reason that numerous Laves phases melted at grain boundaries and microcracks nucleated in the molten pool. The suitable solution treatment temperature of this alloy was 1200 °C.
Key words: as-cast alloy 625; solution treatment; microstructure; tensile properties; γ/Laves eutectic

1 Introduction

Nowadays, the world faces global warming and energy shortage issues, which make it a priority to reduce greenhouse gas emissions and improve energy conversion efficiency [1,2]. To achieve this aim, the next generation of advanced ultra-supercritical (A-USC) power plants must operate at service temperature between 700 and 760 °C and steam pressure up to 35 MPa [3]. The increased operating parameters require that the high temperature materials have better properties, such as creep strength and oxidation resistance. However, the currently used conventional ferritic steels and other alloys [4,5] can hardly meet the requirements, thus they are supposed to be replaced by Ni-based superalloys which exhibit excellent corrosion resistance and mechanical properties. In order to satisfy the requirement of A-USC power plants, a Ni-based as-cast alloy 625 is developed based on Inconel 625 and is now regarded as one of the most promising candidate superalloys.

As an important part of steam turbine, cylinder and valve body are usually under pressure and high temperature environment. Because of their large size and complex geometric characteristics, they are usually molded by casting. This Ni-based as-cast alloy 625 is selected as the candidate material for cylinder and valve body because its excellent casting processability and weldability [6,7]. As the candidate material for cylinder and valve body, the effect of heat treatment on its microstructure and mechanical properties needs to be studied. However, the related research of such large-scale casting is rarely reported.

Generally speaking, the more homogenous the composition is, the closer the incipient melting

Corresponding author: Lan-zhang ZHOU, Tel: +86-24-23971911, E-mail: lzz@imr.ac.cn;
Jie-shan HOU, Tel: +86-24-83978469, E-mail: jshou@imr.ac.cn
DOI: 10.1016/S1003-6326(21)65507-3

temperature will be to the true solidus [8]. That is, the incipient melting temperature can therefore be raised by careful homogenization. The solution temperature range thus must theoretically be defined by the solvus and solidus temperatures of the investigated alloy, and must be carefully studied to allow for segregation. In this way, a relatively uniform composition can be achieved; meanwhile, the residual chemical composition is not too detrimental. Furthermore, the heat-treated microstructure of a superalloy is significantly affected by temperature commonly. For the purpose of further optimization of this cast alloy, detailed investigations on the effect of solution temperature on the microstructure and mechanical properties are required. Thus, in this work an experimental basis for appropriate heat treatment schedule for the as-cast alloy 625 was provided.

2 Experimental

In the present investigation, the alloy was manufactured by in a 25 kg vacuum induction furnace and cast into tensile samples. The nominal chemical composition of the as-cast alloy 625 (in mass fraction) is as follows: 20%−23% Cr, 8%−10% Mo, 3.15%− 4.15% Nb, 0.4% Al, 0.4% Ti, 0.05% C, 0.5% Si, 0.5% Mn, and balanced Ni. The solution treatment temperatures of this alloy were 1050, 1100, 1150, 1175, 1200, 1225 and 1250 °C, respectively. The holding time was 1 h, followed by water quenching.

Specimens for the mechanical tests were machined from the tensile samples after solution treatment under different conditions. The dimensions of the specimens for the tensile tests were 25 mm in gauge length and 5 mm in diameter. The specimens were tested at room temperature on an AG−100KNG DSC−25J machine. The high temperature tensile test at 700 °C was carried out at a strain rate of $10^{-3}s^{-1}$ on a Shimadzu AG−250KNE machine. The value of mechanical properties was the average of tensile results of two specimens. The characterization of the microstructures was conducted on a JEOL 6340 field emission gun scanning electron microscope (SEM) equipped with energy dispersive X-ray spectroscopy (EDS) and Shimadzu 1610 electron probe micro-analyzer (EPMA). The metallographic samples were prepared by mechanical polishing. The observation of the microstructure was carried out using chemical etching with a solution containing 50 vol.% H_2O_2 and 50 vol.% HCl, and the etching time was 40−60 s. The fracture surface of tensile specimens was analyzed by SEM to determine the fracture mechanism of the alloy. The contents of elements in interdendritic regions and dendrite regions were measured by EDS. The segregation ratio of each element was calculated and the results were the average of 10 sets of data. EPMA was used to determine the distribution of elements in the precipitated phase. In order to determine the solidification sequence and the phase transition temperature of this alloy, the DTA test was carried out on a SETSYS evolution 18 integrated thermal analyzer with a heating rate of 10 °C/min in the range of 1100−1450 °C, and argon was the protective atmosphere. The area fraction of precipitations was counted by Image-Pro Plus software and the value was the average of 15 SEM photos. The influence of heat treatment on elemental distribution behavior was studied by thermodynamic software JMatPro with Ni-database.

3 Results and discussion

3.1 Thermodynamic calculation

The thermodynamic method was used to investigate the effect of heat treatment on elemental distribution behavior in the Ni−Nb−Cr−Mo alloy. The basic principle is as follows: (1) the Gibbs free energy G reaches the minimum, and (2) chemical potential of composition in each phase i is equal. The minimum Gibbs free energy G_m is expressed as

$$G_m=\sum_i x_i G_i^0+RT\sum_i x_i\ln x_i+\sum_i\sum_{j>i}x_i x_j\sum_v \Omega_v(x_i-x_j)^v$$

where x_i and x_j are mole fractions of compositions i and j, respectively, G_i^0 is the Gibbs free energy of component i, T is the thermodynamic temperature, R is the molar gas constant, and Ω_v is the interaction coefficient, which has different expressions depending on solid solution, order phase, and intermetallic, and v is the number of interaction systems. A thermodynamic based software, JMatPro with Ni-database [9−11], was used to simulate some of the potential chemical compositions. It is a mature simulation software that is used to calculate

physical properties and phase content at equilibrium state with database of similar alloys, based on thermodynamic formulas and statistic models.

The calculated results of influence of solution temperature on elemental distribution behavior between dendrites cores and interdendritic regions are shown in Fig. 1. The abscissa in the figure represents the distance from the dendrite core to the interdendritic regions. It can be seen that the segregation of Al, Cr, Mo, Nb and Ti decreases in varying degrees after 1 h of solution heat treatment at different temperatures. In the temperature range of 1150−1250 °C, the segregation of the elements decreases gradually with the increase of solution temperature compared with that of as-cast alloy and reaches a minimum at 1250 °C. In other words, the higher the solution temperature is, the more favorable the homogenization of the alloy is.

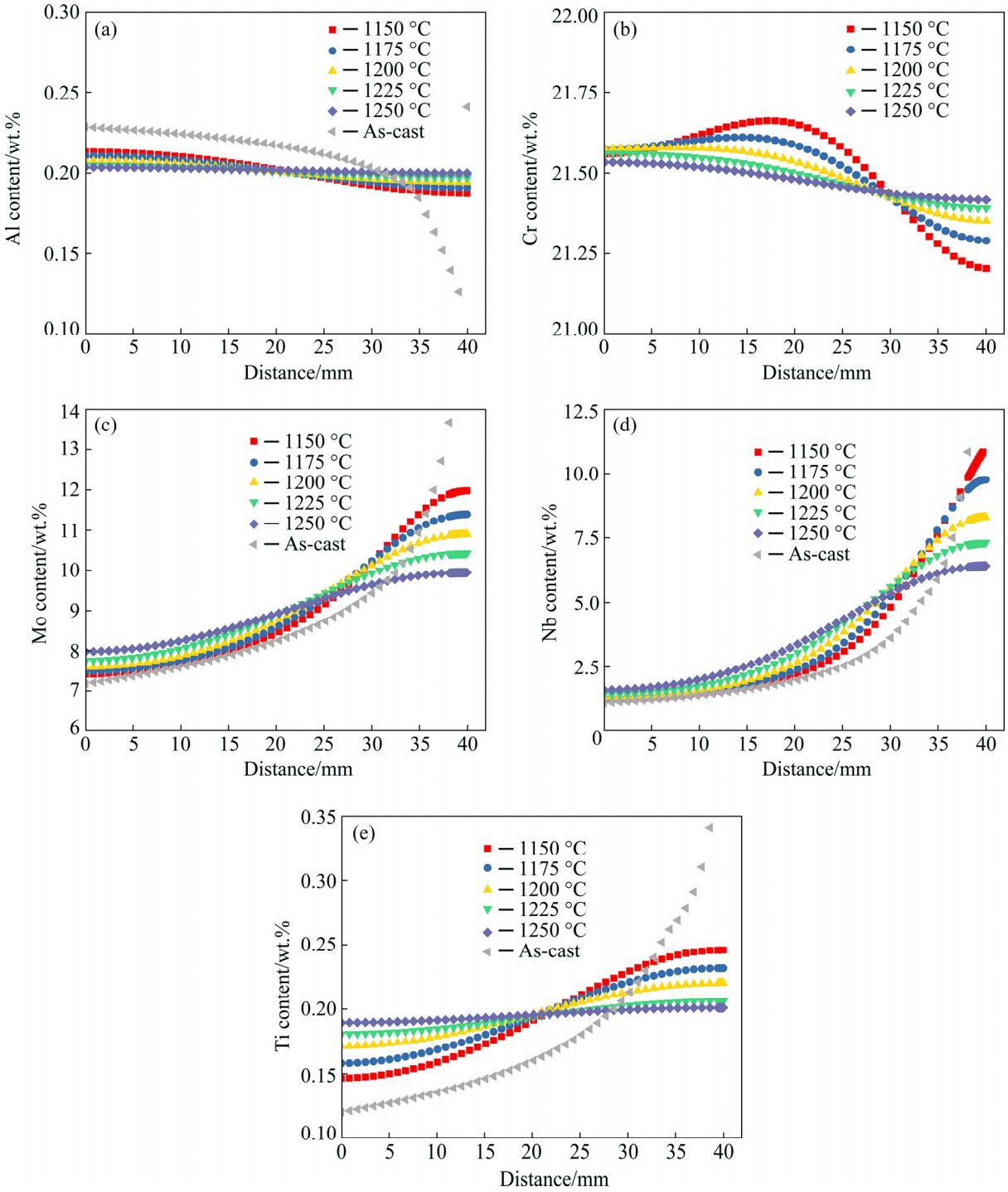

Fig. 1 Calculated results of elements segregation after different solution treatments at different temperatures for 1 h: (a) Al; (b) Cr; (c) Mo; (d) Nb; (e) Ti

However, excessive solution temperature will probably destroy the microstructure of the alloy and have a negative impact on mechanical properties, which may not be shown in the thermal calculation.

3.2 As-cast microstructure

The as-cast Ni-based alloy 625 exhibits a typical dendritic microstructure with dark regions being dendrites cores and bright regions being interdendritic regions, as shown in Fig. 2(a). The secondary dendrite arm spacing is about 65 μm. It can be seen that the dendrite segregation occurs in the as-cast alloy due to the solute atoms redistribution in the solidification process [12]. The degree of dendrite segregation can be characterized by elemental segregation ratio S_R. An element can be judged as a positive segregation element if S_R is greater than 1, otherwise it is a negative segregation element. The segregation ratio of each element in the as-cast alloy is the average value of 10 sets of EDS results, as shown in Table 1. It can be seen that Al is the negative segregation element, while Mo, Ti, Si and Nb are positive segregation elements. Besides, the S_R value of Nb is the largest, which indicates that the segregation of Nb element is the severest and this phenomenon is in good agreement with the experiment results in Ref. [13].

As shown in Fig. 2(b), the main precipitates of the as-cast alloy are blocky or strip-like MC and γ/Laves eutectics which are distributed in the interdendritic regions. The EPMA results show that the carbides are rich in Nb and Ti (Fig. 3). According to the statistical results, the area fraction of carbides is 0.56%. Figure 2(c) shows high magnification morphology of the γ/Laves eutectics of which in the shape is mesh-like and the size is around 18 μm. The γ/Laves eutectics are rich in Si, Mo and Nb (Fig. 3), and area fraction of γ/Laves eutectics is 0.28%. Laves phase is a detrimental phase, and the needle-like and lamellar Laves phases are often the channels of crack nucleus and expansion, which can lead to a significant reduction in the stress rupture strength and room temperature ductility. The granular Laves phase has no significant effect on mechanical properties if the number of Laves phase is limited. On the contrary, if the quantity of Laves phase increases to some extent, the properties will have a decline regardless of the shape of Laves phase [14]. The γ/Laves eutectic is a low melting eutectic phase formed at the end of the solidification, the formation of γ/Laves eutectic is due to the segregation of elements such as Nb, and incipient melting occurs easily during heat treatment process. Moreover, a large amount of Nb and Mo elements are consumed during the formation of γ/Laves eutectic, which reduces the solution strengthening effect of the alloy. As a consequence, the mechanical properties of as-cast alloy are reduced [15,16].

It can be found that a small quantity of MC carbides grow near the γ/Laves eutectic, as shown in Fig. 3. The MC carbides attached to the edge of the Laves phase may be the decomposition products of the alloy during the solidification stage [17].

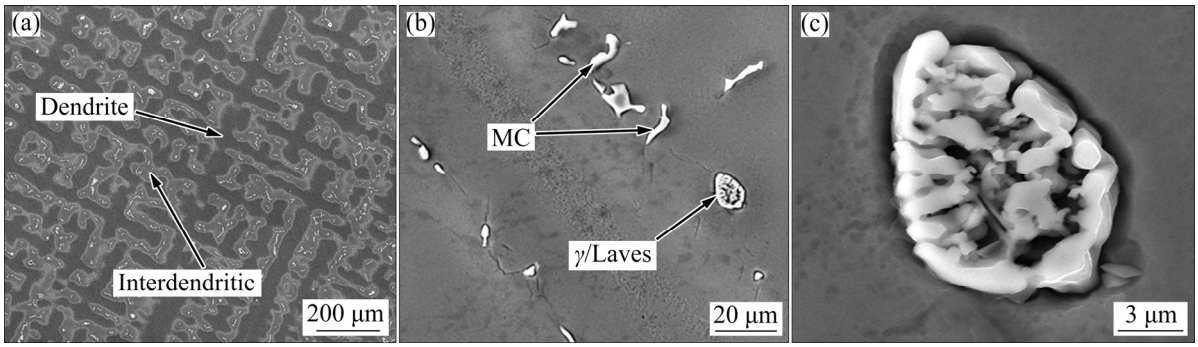

Fig. 2 Typical microstructures of as-cast alloy: (a) Dendrite morphology of as-cast specimen; (b) MC carbides and γ/Laves eutectics; (c) High magnification morphology of γ/Laves eutectics

Table 1 Segregation ratio S_R of major elements in as-cast alloy

Element	Al	Cr	Mo	Ti	Si	Nb	Ni
S_R	0.84	0.93	1.27	1.31	1.35	1.91	0.96

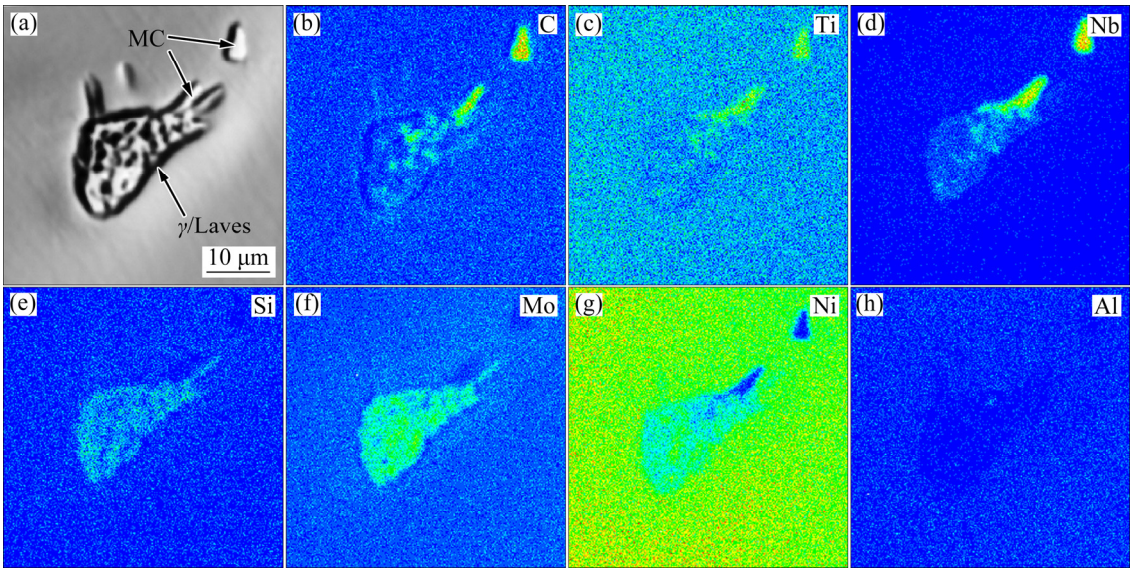

Fig. 3 BSEM image (a) and EPMA element distribution maps (b−h) of γ/Laves eutectic and MC carbides

CAO et al [18] reported that in the process of solidification, the Gibbs free energy change will decrease rapidly when the temperature reaches Laves phase formation temperature, and the formation activation energy of Laves phase at this stage is significantly smaller than that of MC carbides. Therefore, the high concentration of Nb element is mainly used for the precipitation and growth of Laves phase at this formation temperature, while the precipitation of Laves phase will inhibit the continuous precipitation and growth of MC carbides. However, there is still a high concentration of Nb remaining in the local area of MC carbides. Consequently, the nucleation and growth of Laves phase occur adjacent to the MC carbide, which forms the combination of MC carbides and Laves phase.

The DTA results show that there are three endothermic peaks on the DTA heating curve of the as-cast alloy (Fig. 4), which correspond to the melting temperatures of the three phases respectively. As indicated by the arrows in Fig. 4, the temperature corresponding to the endothermic peak at Point A is the phase transition temperature of γ matrix, that is, the liquidus temperature is 1349 °C. The solidus temperature is determined by the intersection of the baseline and the tangent at the maximum slope on the curve, which is deduced that the solidus temperature is 1294 °C. Accordingly, the temperature corresponding to the endothermic peak at Point B is the melting temperature of MC carbides and the temperature at Point C is the incipient melting temperature of γ/Laves eutectic. Therefore, the solidification order of this alloy can be determined as $L \rightarrow L+\gamma \rightarrow L+\gamma+\mathrm{MC} \rightarrow L+\gamma+\mathrm{MC}+\gamma/\mathrm{Laves} \rightarrow \gamma+\mathrm{MC}+\gamma/\mathrm{Laves}$. Such solidification feature has been reported in Ref. [13] and similar solidification behavior is also present in Ni-based superalloys such as In718 [16].

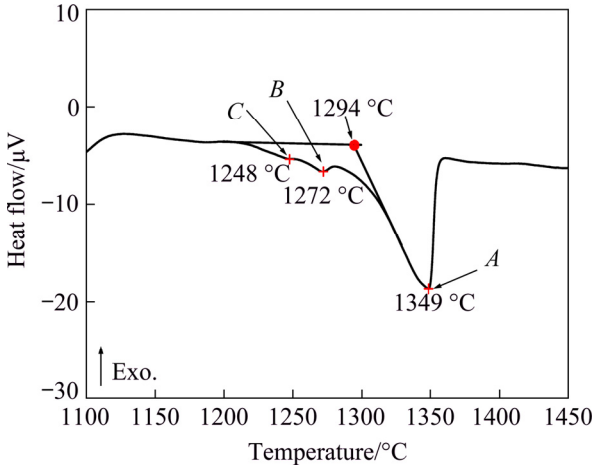

Fig. 4 DTA heating curve of as-cast alloy

3.3 Heat-treated microstructure

The microstructures of alloy after solution treatment at different temperatures are shown in Fig. 5. The EDS results indicate that the primary MC carbides remain intact after solution treatment. The solution temperature has little influence on the distribution and morphology of MC carbides when

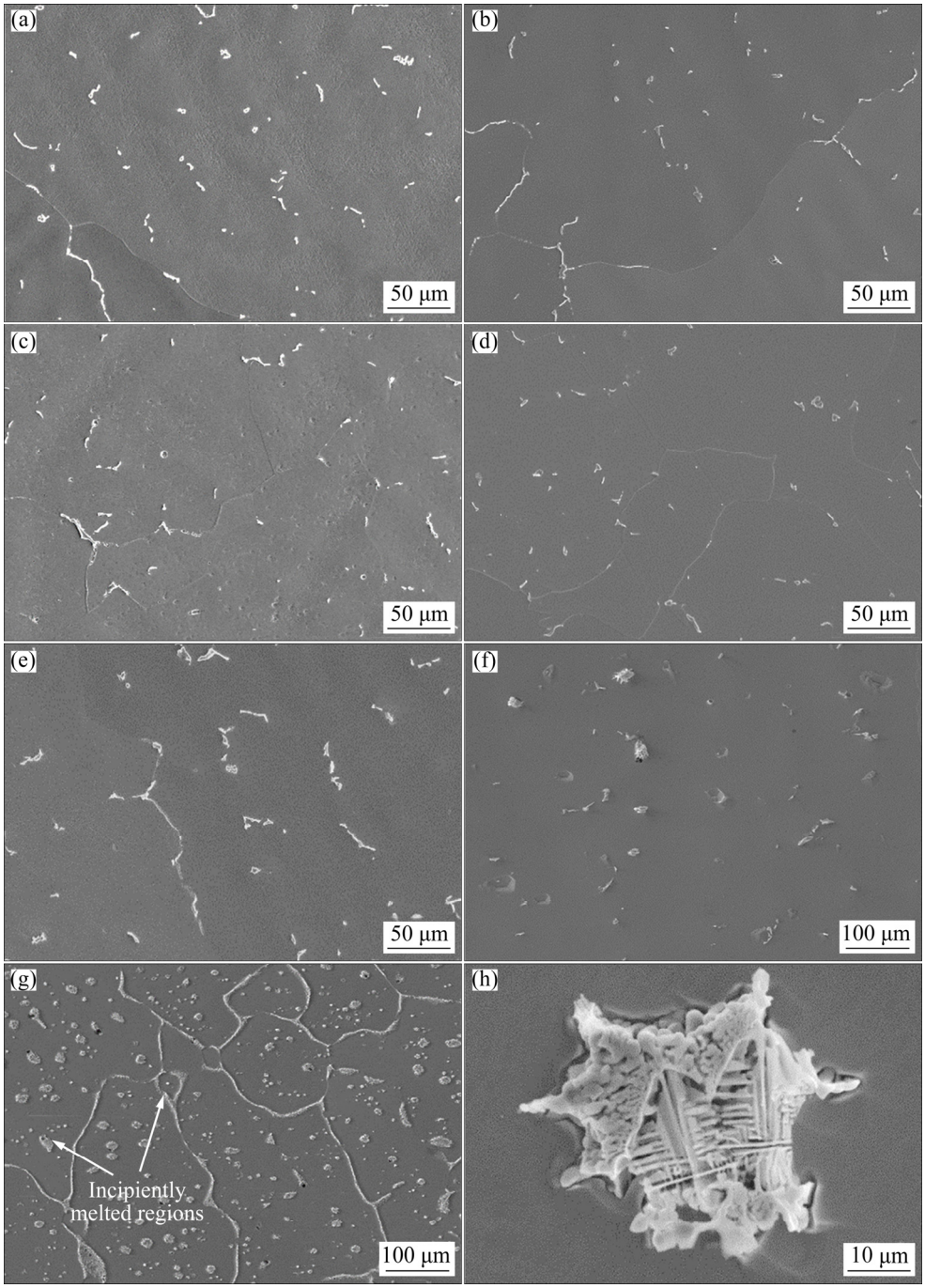

Fig. 5 Microstructures of alloy after solution treatment at 1050 °C (a), 1100 °C (b), 1150 °C (c), 1175 °C (d), 1200 °C (e), 1225 °C (f), 1250 °C (g) and morphology of molten pool (h)

the temperature is between 1050 and 1200 °C. Besides, the redissolution of partial *γ*/Laves eutectics occurs and their shapes are transformed from mesh-like to block-like. The morphology and EDS spectrum of Laves phase are shown in Fig. 6. Since the shape of Laves phase is similar to that of MC carbides, it is hard to be distinguished accurately by their appearance. Hence, the quantitative analysis of the two phases is difficult.

The nature of the solution is to improve the homogeneous degree of the alloy's composition by interdiffusion between elements. According to Arrhenius equation [19], temperature is the main factor affecting the diffusion of elements. The diffusion rate and solubility of the elements in the matrix increase with the increase of the solution temperature. The precipitates in the alloy are difficult to quantitatively analyze with the change of the solution temperature, since there exists the phenomenon of the dissolution of Laves phase and

carbides in the solution process. The dissolution temperatures of Laves phase are different in different alloys. The Laves phase in GH4151 alloy has been completely dissolved at 1150 °C [20] while the corresponding temperature is 1160 °C in IN706 alloy [21].

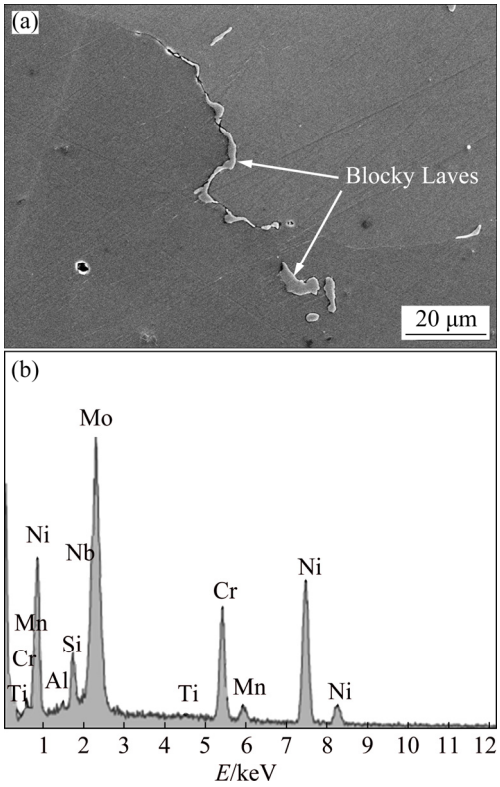

Fig. 6 SEM image of Laves phase (a) and corresponding EDS spectrum (b)

Figures 5(f) and (g) show that the dissolution of MC carbides and Laves phase is more obvious after solution treatment at 1225 and 1250 °C compared with that of the alloy treated at other solution temperatures. The amount of MC carbides is reduced and its shape becomes block-like gradually after solution treatment at 1225 °C. Furthermore, the incipient melting of the low melting point *γ*/Laves eutectic occurs with isolated molten pool forming mutually in the grain interior, and the area fraction of *γ*/Laves eutectic is about 0.43%. The results indicate that the incipient melting temperature of *γ*/Laves eutectic is between 1200 and 1225 °C, which is different from the DTA results. This difference is ascribed to the fact that the sensitivity of the recorder is not high enough in the case of continuous heating, and the heat produced by a small amount of liquid cannot be fully reflected, which resulted in the phase transition lagging behind the recorded temperature. The incipient melting in superalloy is harmful to its hot workability [22] and seriously reduces its stress rupture life [23−25].

As the solution temperature increases to 1250 °C, the number of incipient melting zones increases obviously with the area fraction reaching 4.13%, and the morphology of molten pool is shown in Fig. 5(h). In this condition, only a small amount of MC carbides exist in the solution-treated microstructure and their shape is granular. It can be seen that grain boundary is covered with continuous and molten Laves phase, which results in the deterioration of mechanical properties. After the formation of incipient melting microstructure, the *γ*/Laves eutectic and a new phase with dendritic structure are formed in the same molten pool (Fig. 5(h)). The reason for the new phase with dendritic structure is the large supercooling of the solid−liquid interface during the water quenching process. As a result, the appearance shows the dendritic structure after crystallization and then part of the dendrites are joined into flakes. The EPMA results of molten pool reveal that the new phase with dendritic structure is MC carbides enriched in Nb and Ti elements, as shown in Fig. 7. Since there exists a competitive growth relationship between Laves phase and MC carbides, Nb element will be released after Laves phase melting and the formation of MC carbides is promoted. There is no single phase formed in molten pool because carbides with high melting point contain more Nb element, and the concentration of Nb in the molten pool is insufficient to facilitate the subsequent formation after the formation of some dendrite phases. The Laves phase with a relatively low Nb content will be formed in residual liquid. The edge of the re-precipitated Laves phase is jagged, while the edge of *γ*/Laves eutectics in the as-cast structure is relatively smooth. Table 2 shows the compositions of Laves phase in the as-cast alloy and molten pool. The results show that the Laves phase is re-precipitated and is different from that in as-cast alloy.

3.4 Mechanical properties

Figure 8 shows the room temperature yield strength (YS), ultimate tensile strength (UTS) and ductility of as-cast alloy after various solution treatments. It can be seen that the effect of solution

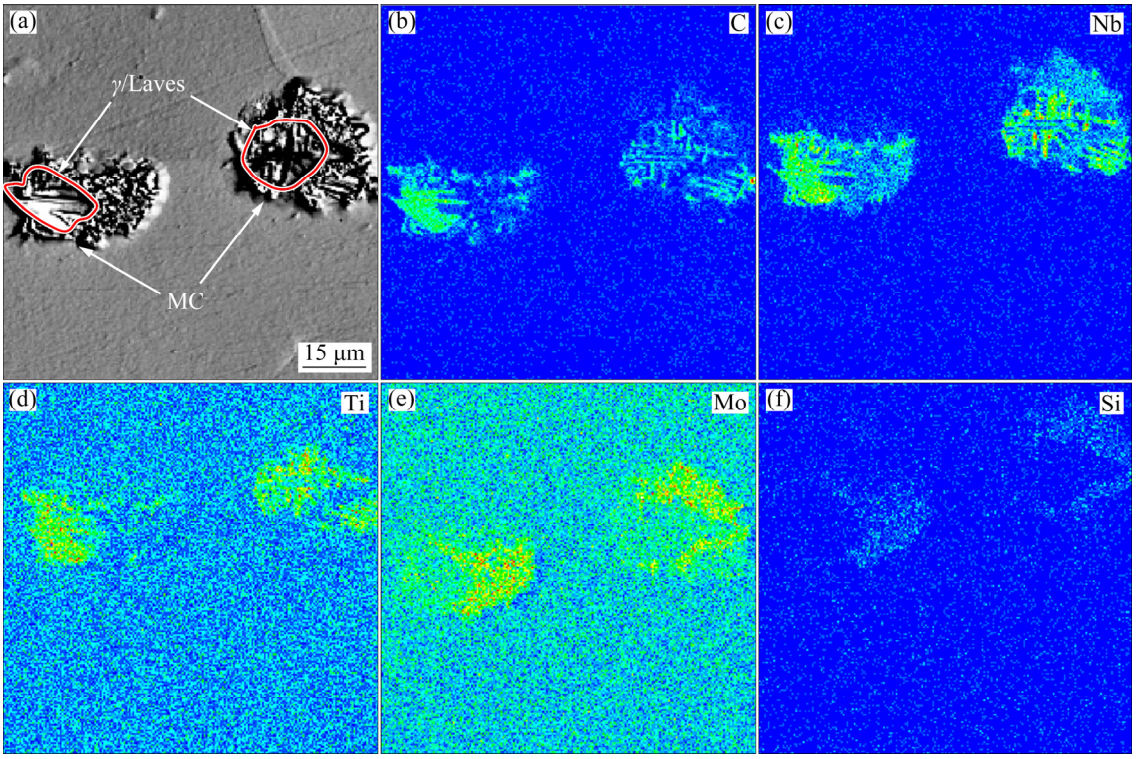

Fig. 7 BSEM image (a) and EPMA element distribution maps (b−f) of incipiently melted region

Table 2 Chemical compositions of Laves phase

Sample	Composition/wt.%							
	Al	Cr	Mo	Ti	Si	Nb	Ni	Mn
As-cast	0.1	12.9	30.2	0.1	4.1	13.9	38.5	0.2
Molten pool	0.1	14.1	22.7	0.2	2.9	19.9	39.8	0.3

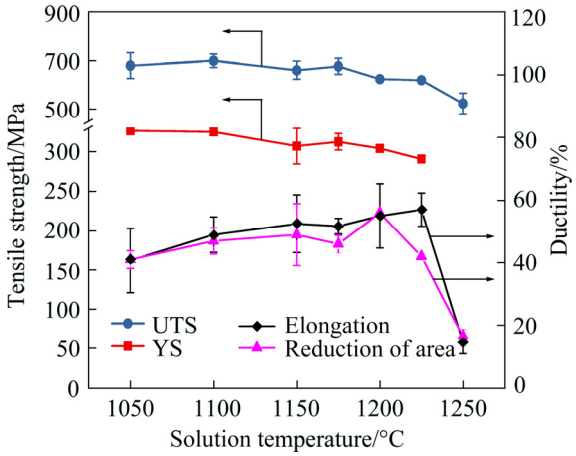

Fig. 8 Effect of solution temperature on tensile strength and ductility of alloy at room temperature

temperature on tensile strength is not very obvious when the solution temperature is below 1225 °C. The yield strength shows an extremely slow downward trend with the increase of solution temperature, and the overall change is relatively small. The ultimate tensile strength is similar to yield strength in addition to the extent of decline and the value is basically maintained at 620−680 MPa. After solution treatment at 1250 °C, the alloy exhibits a minimum in UTS compared with the solution treatment at other temperatures. The reduction is mainly derived from the presence of numerous incipient melting Laves phases. The main reasons for the above results can be understood from the following two aspects. On one hand, with the increase of area fraction of incipient melting zones, the consumption of solution strengthening elements such as Mo gradually increases. Thereby, the effect of solution strengthening is weakened and the tensile strength has a decline. On the other hand, the binding force between the flake-like MC carbides and matrix is lower, and the cracks will be formed at the interface between MC carbides and matrix when the external force is exerted. Besides, a continuous incipient melting Laves phase at grain boundary will cause the deterioration of tensile properties. Hence, the incipient melting zone is the key factor affecting the mechanical properties.

When the solution temperature is lower than

1225 °C, the ductility has an apparent improvement with the increase of solution temperature. However, the ductility of the alloy has a huge drop after solution treatment at 1250 °C. Figure 9 shows the microstructures of fracture surface and longitudinal sections near fracture. After solution at 1050−1225 °C, the fracture surface morphology of the alloy shows a typical dendrite fracture feature, as shown in Fig. 9(a). The necking phenomenon is obvious in the vicinity of fracture and the fracture displays cup- and cone-shape, and the cracks initiate from the center of sample and expand outward. The crack source and extension area are obvious, and the shear lips and tear edges can be observed. Moreover, it can be found that considerable dimples on cleavage surfaces and small granular MC carbides are present at the bottom of the dimples (Fig. 9(b)). In the process of plastic deformation, there is a high stress concentration at the interface between MC carbides and matrix, which causes the carbides to break or peel off from the matrix to form microvoids. Figure 9(c) shows that the fracture surface is flatter after solution treatment at 1200 °C and the dendritic fracture characteristic is no longer obvious compared with the fracture surface after solution treatment at 1150 °C. Figure 9(d) reveals the micrograph of longitudinal sections near the fracture. It can be seen that a certain amount of secondary cracks are present in the grain interior and at grain boundary. Hence, the fracture model is microvoid aggregation type transgranular fracture caused by the growth and junction of microvoids. The ability of atom diffusion is enhanced and the uniformity of grain internal composition is improved with the increase of solution temperature,

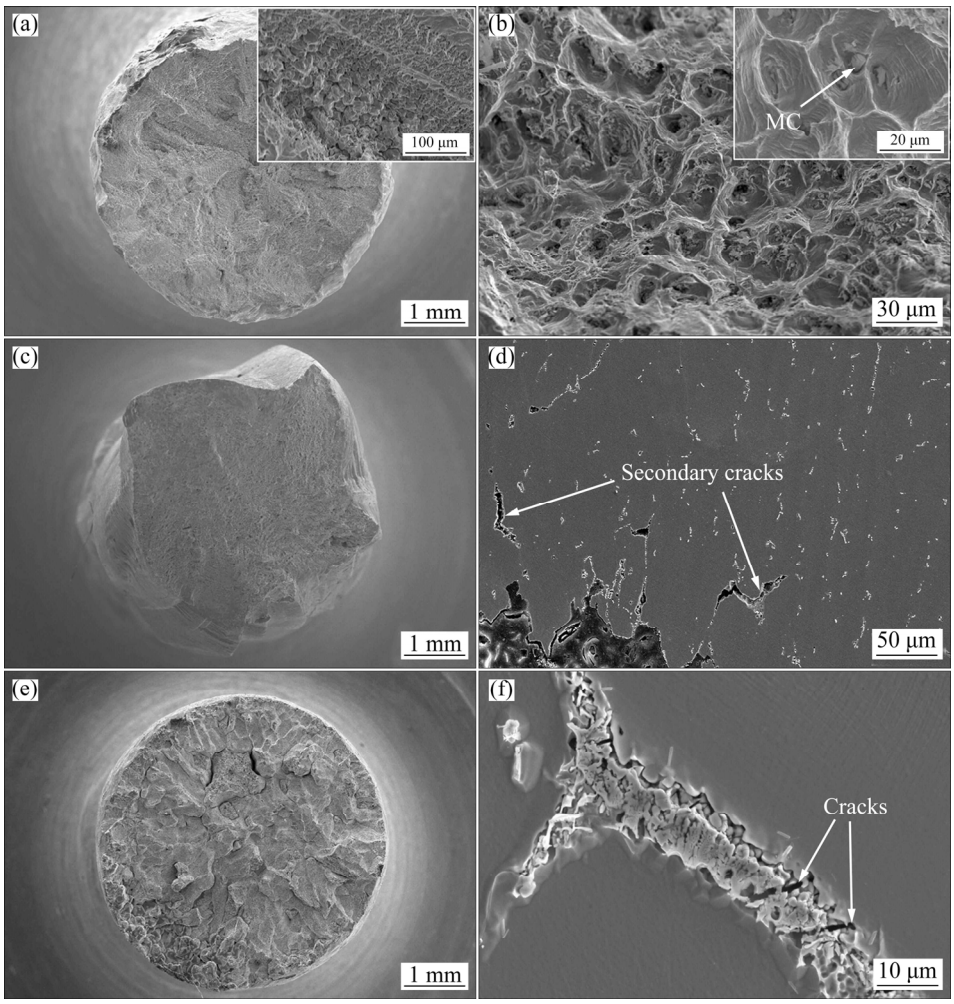

Fig. 9 Micrographs of fracture surface and longitudinal sections near fracture: (a) Fracture surface after solution treatment at 1150 °C; (b) Microstructure of fracture surface; (c) Fracture surface after solution treatment at 1200 °C; (d) Microstructure of longitudinal section near fracture; (e) Fracture surface after solution treatment at 1250 °C; (f) Microstructure of grain boundary

which results in the decrease of the dendrite segregation. Simultaneously, the degree of dissolution of MC carbides and Laves phase increases with the increase of solution temperature, which leads to a decline in their resistance to dislocation motion. Moreover, at higher temperature, the dislocation movement velocity in the alloy is faster and the annihilation of these dislocations occurs. This may be another important reason to improve the plastic deformation capacity of the alloy.

After solution treatment at 1250 °C, the alloy has a sharp drop in ductility. Figure 9(e) shows the fracture surface of the alloy. It is observed that the alloy exhibits an apparent feature of intergranular fracture. Intergranular fracture occurs because strength of grain boundary is lower than that of grain interior. Besides, no obvious necking phenomenon can be observed, which suggests that the ductility of the alloy after solution treatment at 1250 °C is poor. The micrographs of longitudinal sections indicate that the secondary cracks are mainly distributed at grain boundary and the cracking of grain boundary eventually leads to the failure. As mentioned in the previous sections, the grain boundary is covered with continuous incipient melting Laves phase (Fig. 5(g)), which leads to the deterioration of mechanical properties. Figure 9(f) demonstrates that the crack initiation and propagation begin from the molten pool. The Laves phase in the incipient melting zones is the brittle phase and has little ability to withstand plastic deformation. The cracks are easily produced at the interface between Laves phase and matrix. In addition, the cracks spread rapidly in the molten pool and can accelerate the fracture process, which leads to the decrease in ductility of the alloy.

Figure 10 shows YS, UTS and ductility of the alloy tested at 700 °C. The results show that the UTS decreases gradually with the solution temperature increasing, and has a minimum after solution treatment at 1250 °C. The ductility increases slowly when the solution temperature is lower than 1225 °C, and it drops to a minimum value at 1250 °C due to the presence of incipient melting Laves phase. The morphology of fracture surface at high temperature is similar to that at room temperature, which is unnecessary to elaborate further.

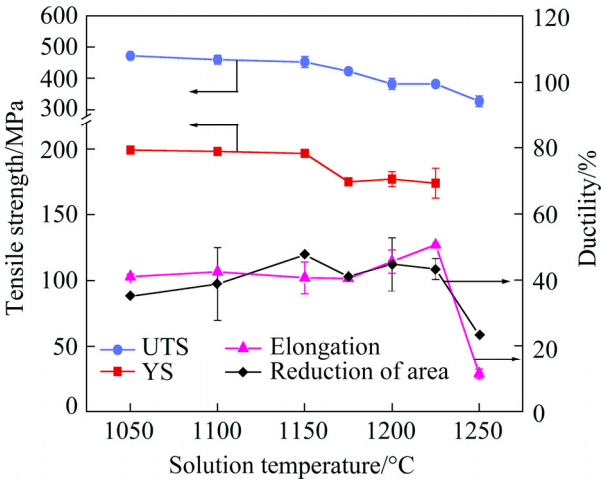

Fig. 10 Effect of solution temperature on tensile strength and ductility of alloy at 700 °C

4 Conclusions

(1) The as-cast alloy exhibits a typical dendrite morphology with the main precipitates including blocky and strip-like MC carbides rich in Nb and Ti, and γ/Laves eutectics are rich in Si, Nb and Mo.

(2) After solution treatment at 1050−1200 °C, the morphology of γ/Laves eutectic transforms from mesh-like shape to blocky shape. After solution treatment at 1225 °C, the redissolution of MC carbides and incipient melting of a small amount of γ/Laves eutectics occur. After solution treatment at 1250 °C, except for a small amount of granular carbides, there exhibit numerous initial melting Laves phases. The Nb- and Ti-rich dendritic MC carbides precipitate after the solidification of molten pool.

(3) The yield strength has no significant change with the increase of solution temperature, while the UTS decreases monotonically. After solution treatment at 1050−1225 °C, the trans-granular fracture is dominated by microvoid aggregation type mechanism. After solution treatment at 1250 °C, both the strength and ductility reach minimum values due to the presence of incipient melting Laves phase and the generation of cracks in molten pool. The suitable solution treatment temperature of cast alloy 625 is 1200 °C.

Acknowledgments

The authors would like to appreciate the financial support from the National Natural Science Foundation of China (51571191).

References

[1] CAU G, TOLA V, DEIANA P. Comparative performance assessment of USC and IGCC power plants integrated with CO_2 capture systems [J]. Fuel, 2014, 11: 820−833.

[2] GUO Yan, LI Tai-jiang, WANG Cai-xia, HOU Shu-fang. Microstructure and phase precipitate behavior of Inconel 740H during aging [J]. Transactions of Nonferrous Metals Society of China, 2016, 26(6): 1598−1606.

[3] WU Q Y, SONG H J, SWINDEMANd R W, SHINGLE-DECKER J P, VASUDEVAN, V K. Microstructure of long-term aged IN617 Ni-base superalloy [J]. Metallurgical and Materials Transaction A, 2008, 39: 2569−2585.

[4] OU Mei-qiong, HAO Xian-chao, MA Ying-che, LIU Rui-chang, ZHANG Long, LIU Kui. Effect of carbon on the microstructure and stress rupture properties of a new Ni−Cr−W−Fe alloy for advanced ultra-supercritical power plants [J]. Journal of Alloys and Compounds, 2018, 732: 107−115.

[5] ZHAO H Q, XIE X S, SMITH G D, SHAILESHl J P. The corrosion of INCONEL alloy 740 in simulated environments for pulverized coal-fired boiler [J]. Materials Chemistry and Physics, 2005, 90: 275−281.

[6] PAVAN A H V, NARAYAN R L, SWAMY M, SINGH K, RAMAMURTY U. Stress rupture embrittlement in cast Ni-based superalloy 625 [J]. Materials Science and Engineering A, 2020, 793: 139811.

[7] MATHEW M D, RAO K B S, MANNAN S L. Creep properties of service-exposed alloy 625 after re-solution annealing treatment [J]. Materials Science and Engineering A, 2004, 372(1−2): 327−333.

[8] DURRAND-CHARRE M. The microstructure of superalloys [M]. Lodon: Taylor Francis Ltd., 1998.

[9] PEI Chuan-hu, FAN Qun-bo, CAI Hong-nian, LI jian-chong. High temperature deformation behavior of the TC6 titanium alloy under the uniform DC electric field [J]. Journal of Alloys and Compounds, 2010, 489: 401−407.

[10] YANG Jian, TIAN Jian-jun, HAO Fei-fei, DAN ting, REN Xue-jun, YANG Yu-lin, YANG Qing-xiang. Microstructure and wear resistance of the hypereutectic Fe−Cr−C alloy hardfacing metals with different La_2O_3 additives [J]. Applied Surface Science, 2014, 289: 437−444.

[11] ZHAO Xin-bao, DANG Ying-ying, YIN Hong-fei, YUAN Yong, LU Jin-tao, YANG Zhen, GU Yue-feng. Evolution of the microstructure and microhardness of a new wrought Ni−Fe based superalloy during high temperature aging [J]. Journal of Alloys and Compounds, 2015, 644: 66−70.

[12] CHEN Fu-yi, JIE Wan-qi. Numerical model and rapid algorithm of solute redistribution in dendritic solidification [J]. The Chinese Journal of Nonferrous Metals, 2016, 26(6): 1598−1606. (in Chinese)

[13] MIN Zhi-xian, SHEN Jun, FENG Zhou-rong, WANG Ling-shui, LIU Lin, FU Heng-zhi. Study on partition ratio and segregation behavior of DZ125 alloy during directional solidification [J]. Acta Metallurgica Sinica, 2010, 46(12): 1543−1548. (in Chinese)

[14] GUO Jian-ting. Materials science and engineering for superalloys [M]. Beijing: Science Press, 2008. (in Chinese)

[15] ZHANG Ke-ren, XIE Fa-qin, HU Rui, WU Xiang-qing. Relationship between microstructure and mechanical properties of undercooled K4169 superalloy [J]. Transactions of Nonferrous Metals Society of China, 2016, 26(7): 1885−1891.

[16] MANIKANDAN S G K, SIVAKUMAR D, PRASAD R K, KAMARAJ M. Laves phase in alloy 718 fusion zone microscopic and calorimetric studies [J]. Materials Characterization, 2015, 100: 192−206.

[17] CIESLAK M J, HEADLEY T J, ROMIG A D, KOLLIE T. A melting and solidification study of alloy 625 [J]. Metallurgical Transactions A, 1988, 19(9): 2319−2331.

[18] CAO Guo-xin, ZHANG Mai-cang, DONG Jian-xin, YAO Zhi-hao, ZHENG Lei. Effects of Nb content variations on precipitates evolution of GH4169 ingots during their solidification and homogenization processes [J]. Rare Metal Materials and Engineering, 2014, 43(1): 103−108. (in Chinese)

[19] KEDDAM M. A kinetic model for the borided layers by the paste-boriding process [J]. Applied Surface Science, 2004, 236(1−4): 451−455.

[20] LI Xin-xu, JIA Chong-lin, ZHANG Yong, LÜ Shao-min, JIANG Zhou-hua. Incipient melting phase and its dissolution kinetics for a new superalloy [J]. Transactions of Nonferrous Metals Society of China, 2020, 30(8): 2107−2118.

[21] ZHANG Sha, XIN Xin, SUN Wen-ru, SUN Xiao-feng, YU Lian-xu, ZHANG Yu-chen, HU Zhuang-qi. Effect of phosphorus segregation on as-cast microstructure and homogenization treatment of IN706 alloy [J]. Transactions of Nonferrous Metals Society of China, 2015, 25(9): 2939−2947.

[22] JAHANGIRI M R, BOUTORABI S M A, ARABI H. Study on incipient melting in cast Ni base IN939 superalloy during solution annealing and its effect on hot workability [J]. Materials Science and Technology, 2012, 28(12): 1402−1413.

[23] SIDHU R K, OJO O A, CHATURVED M C. Sub-solidus melting of directionally solidified Rene 80 superalloy during solution heat treatment [J]. Journal of Materials Science, 2008, 43(10): 3612−3617.

[24] LEE H S, KIM D H, KIM D S, YOO K B. Microstructural changes by heat treatment for single crystal superalloy exposed at high temperature [J]. Journal of Alloys and Compounds, 2013, 561: 135−141.

[25] MOSTAFAEI M, ABBASI S M. Influence of Zr content on the incipient melting behavior and stress-rupture life of CM247 LC nickel base superalloy [J]. Journal of Alloys and Compounds, 2015, 648: 1031−1037.

固溶处理对铸造 625 合金显微组织和拉伸性能的影响

杨 飞[1,2]，侯介山[1]，王常帅[1]，周兰章[1]

1. 中国科学院 金属研究所，沈阳 110016；
2. 中国科学技术大学 材料科学与工程学院，合肥 230026

摘 要：研究 1050~1250 °C 固溶处理对铸造 625 合金显微组织和拉伸性能的影响。采用 SEM、EDS、EPMA 和 DTA 研究合金的显微组织及凝固特征。结果表明，合金的凝固顺序为 $L\rightarrow L+\gamma\rightarrow L+\gamma+\text{MC}\rightarrow L+\gamma+\text{MC}+\gamma/\text{Laves}\rightarrow \gamma+\text{MC}+\gamma/\text{Laves}$。经 1225 和 1250 °C 固溶处理后，组织中 Laves 相发生初熔。经不同温度固溶处理后，合金的极限抗拉强度随固溶温度的升高而降低，屈服强度则无明显变化；伸长率随固溶温度升高先略微增加，在 1250 °C 达到最小值。经 1250 °C 固溶处理后，合金断裂机制由穿晶断裂转变为沿晶断裂，主要原因为晶界上大量的 Laves 相熔化，微裂纹在熔池中大量萌生。该合金的最佳固溶处理温度为 1200 °C。

关键词：铸造 625 合金；固溶处理；显微组织；拉伸性能；γ/Laves 共晶

(Edited by Wei-ping CHEN)